




Effect of Non-Darcy Flow in Transient Pressure Behavior with Poroelastic Dual-Permeability After-Closure Analysis of Fracture Test

Gregory L. G. Zuñiga Arenas, Student¹ , Joseph Sinchitullo, M.Sc.¹ , Eduardo Calle Contreras, Student¹ 

¹Universidad Nacional de Ingeniería, Peru, gregory.zuniga.a@uni.pe, jsinchitullo@uni.pe, ecallec@uni.pe

Abstract—Non-Darcy flow is introduced to analyze the wellbore dual-pressure responses for naturally fractured reservoirs. The pressure decline is assessed using dual-porosity/dual-permeability poroelastic theory during the post-closure (after-closure) phase of impulse-fracture tests. This analysis reveals that parameters for both matrix and fracture can be estimated based on identified dual-flow regimes. The wellbore pressure behavior is depicted in a log-log pressure plot, where the transition period between pseudolinear and pseudoradial regimes is examined. The log-log plot of pressure indicates that non-Darcy flow significantly impacts the transition period, resulting in a narrower and steeper curve. Moreover, it shows a slight convex shape in the pseudoradial flow region. The semianalytical expressions are provided to estimate these parameters in the limit regions for the dual-flow regimes. Finally, the study also performs a sensitivity analysis and compares the semianalytical solution in limiting cases where Darcy flow in the fracture system is compared.

Index Terms—Non-Darcy Flow, Transient Pressure, Poroelastic, Dual-Permeability, Fracture Test

I. INTRODUCTION

Forchheimer equation takes into account the deviation from linearity in Darcy's law when the flow rate is high. This is particularly important in hydraulic fracture conductivity, where the flow rate in the fracture is exceedingly higher than in the reservoir matrix [1]. Therefore, is expected to be non-negligible inertial losses and introduces the inertial factor (β) in the Forchheimer equation.

Studies for modeling non-Darcy flow in naturally fractured reservoirs are limited. Choi et al. [2] used the Forchheimer form of flow equation to model fracture flow in a dual-porosity/dual-permeability model. They simulated their numerical model and observed the variation of fracture properties. Other studies also highlight the significant impact of the fluid flow through the fracture on pressure behavior, especially on early pressure responses [3], [4].

In all cases, naturally fractured formations are modeled by an idealized dual porosity model. In addition, the after closure analysis can be applied over a poroelastic model accounting for both fracture and matrix fluid flow to the wellbore. Liu et al. [5] employed the poroelastic model for a dual-porosity/dual-permeability case, considering interporosity flow

between matrix and fracture. To solve the model, they employed the line-source theory and Darcy flow in the matrix and fracture.

This research extends Liu et al. [5]'s model to account for the non-Darcy flow over the fracture. A semi-analytical solution is then applied to simulate the after-closure pressure decline and allows the identification of natural fractures and flow regimes in the formation. The reservoir is discretized into segments in the radial domain to handle the non-linearity of Forchheimer equation [6].

II. MODEL FORMULATION

To simulate an impulse-fracture test, it is considered a fracturing fluid pumped at a rate Q_0 for a time t_p . The created hydraulic fracture closes at time t_c . For a horizontal plane in the formation, the wellbore will represent a point and its after-closure pressure can be simulated by a line-source solution (see Figure 1). Therefore, the pressure in both matrix and fracture responses will be simulated.

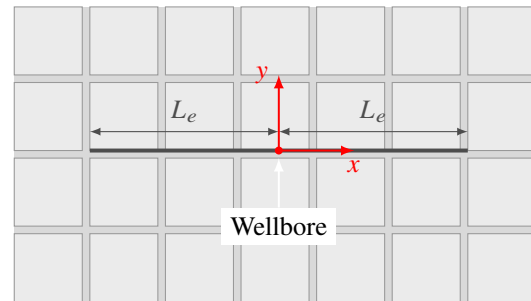


Figure 1. Line-source simulation in an idealized naturally fractured rock formation.

A. Dual Poroelastic Approach

The poroelastic dual-permeability approach employs the linear isotropic constitutive equations for the naturally fractured rock formation as:

$$\sigma_{ij} = \left(\bar{K} - \frac{2}{3} \bar{G} \right) \varepsilon \delta_{ij} + 2 \bar{G} \varepsilon_{ij} + \left(\bar{\alpha}^I p^I + \bar{\alpha}^II p^{II} \right) \delta_{ij}, \quad (1)$$

$$\zeta^I = -\bar{\alpha}^I \varepsilon + \frac{p^I}{M^I} + \frac{p^{II}}{M^{I,II}}, \quad (2)$$

$$\zeta^{II} = -\bar{\alpha}^{II} \varepsilon + \frac{p^I}{M^{I,II}} + \frac{p^{II}}{M^{II}}, \quad (3)$$

Digital Object Identifier: (only for full papers, inserted by LACCEI).
ISSN, ISBN: (to be inserted by LACCEI).
DO NOT REMOVE

where I and II refer to the rock matrix and fractures medium, respectively; \bar{K} and \bar{G} are the overall bulk and shear modulus, respectively; $\bar{\alpha}$ is the effective-pore-pressure coefficient of the medium; p is the matrix or fracture-pore pressure; ζ is the variation of total fluid contents; and \bar{M} is the effective coupled Biot moduli.

B. Darcy and Non-Darcy Flow Behavior

In the matrix, the presence of inertial effects is relatively minor as a result of the low velocities observed. Conversely, within the fractures, the inertial effects can become highly significant due to the considerably higher velocities reached in this particular domain. The latter can lead to significant non-Darcy flow effects at least in the near wellbore region [7].

$$q_i^I = -\frac{k^I}{\mu} \frac{\partial p^I}{\partial x_i}, \quad (4)$$

$$q_i^{II} = -\frac{k^{II}}{\mu} \frac{\partial p^{II}}{\partial x_i} - \frac{\rho\beta}{\mu} q^{II} q_i^{II}, \quad (5)$$

where k is the permeability of the medium, μ is the fluid viscosity, ρ is the fluid density, and β is the non-Darcy flow coefficient or the Forchheimer inertial resistance coefficient.

C. Other Governing Equations

The next governing equations are:

- Equilibrium equation,

$$\frac{\partial \sigma_{ij}}{\partial x_i} = 0; \quad (6)$$

- Strain-displacement relation,

$$\varepsilon_{ij} = \frac{1}{2} \left(\frac{\partial u_i}{\partial x_j} + \frac{\partial u_j}{\partial x_i} \right); \quad (7)$$

- Fluid-continuity equations,

$$\frac{\partial \zeta^I}{\partial t} = -v^I \frac{\partial q_i^I}{\partial x_i} + \Gamma, \quad (8)$$

$$\frac{\partial \zeta^{II}}{\partial t} = -v^{II} \frac{\partial q_i^{II}}{\partial x_i} - \Gamma; \quad (9)$$

where v is the bulk-volume fraction of the medium, and Γ is the inter-porosity-fluid-flux transfer.

The inter-porosity-fluid-flow is modeled proportional to the pressure differences between two overlapping regions of porous media,

$$\Gamma = \lambda(p^{II} - p^I). \quad (10)$$

D. Semi-analytical Procedure

To handle the non-linearity of Forchheimer equation, a dimensionless non-Darcy modifier is defined as follows:

$$\delta = \frac{1}{1 + \frac{\rho\beta}{\mu} q^{II}} \quad (11)$$

which is a function of radius and time.

- 1) *Reservoir Gridding*: Reservoir discretization is used to handle the non-linear term in Equation (19) (i.e. δ) with a stepwise function. Through this simplification, δ becomes independent of space coordinates. So, in the reservoir discretized reservoir system, δ is approximated by its average value $\delta(t)$.
- 2) *Algorithm*: To deal with δ variation in time, a pseudo-time is defined as

$$\tau = \int_0^t \delta(\zeta) d\zeta. \quad (12)$$

To compute the pseudo-time, fluid flux must be given. Therefore, Zeng [8] presented an iterative procedure as follows:

- 1) $\delta(t)$ is assumed to be 1, which means that fluid flux is calculated based on Darcy flow results;
- 2) $\delta(t)$ value is then updated and the pseudo-time is calculated with Equation (11);
- 3) The new fluid flux is computed based on the results obtained with the purposed methodology (see Appendix A);
- 4) If the $\delta(t)$ value is not converged, steps 2–4 must be repeated, otherwise proceed with the subsequent time (see Appendix B).

III. RESULTS

In this section, the numerical example of Liu et al. [5] will be contrasted against the results of the non-Darcy results. The parameters in Table I are selected to test the pressure response of the Woodford shale under the same assumptions of the authors.

The hydraulic-treatment-simulation data employed is described below:

- Pump rate, $Q_0 = 0.008 \text{ m}^3/\text{s}$;
- Pump time, $t_p = 6 \text{ min}$;
- Fracture-closure time, $t_c = 8 \text{ min}$;
- Fracture height, $H = 10 \text{ m}$;
- Equivalent half-fracture length, $L_e = 25 \text{ m}$.

The simulation was performed in python, using the libraries Sympy and mpmath to code the symbolic computation needed for the simulation of the finite interval line source solution. To perform the numerical inverse Laplace transform, mpmath offers various algorithms including: Stehfest, Talbot, Cohen, etc; and match the results with the fastest and most accurate solution. In contrast with Wolfram Mathematica (used in [5]), employing an open source programming language allows a better user interaction and computing times, even when python was not designed to perform symbolic computation.

Figure 2 gives the log-log pressure plots of the matrix and fractures under Darcy-flow condition, $\delta = 1$. This result is in agreement with the simulation performed in Liu et al. [5]. The good match of matrix- and fracture-pressure responses

Table I
ROCK AND FLUID PARAMETERS

Parameters	K (GPa)	ν	B	α	k (nD)	μ (cP)	ν (%)	λ (MPa ⁻¹ d ⁻¹)	ρ (g cm ⁻³)	β (m ⁻¹)
Matrix (I)	4.8	0.3	0.56	0.88	45	1	99	1×10^{-5}	1	—
Fracture (II)	0.096	0.3	0.96	0.9	1×10^5	1	1	—	—	const

showed in this figure suggest the accuracy and validity of the semi-analytical model.

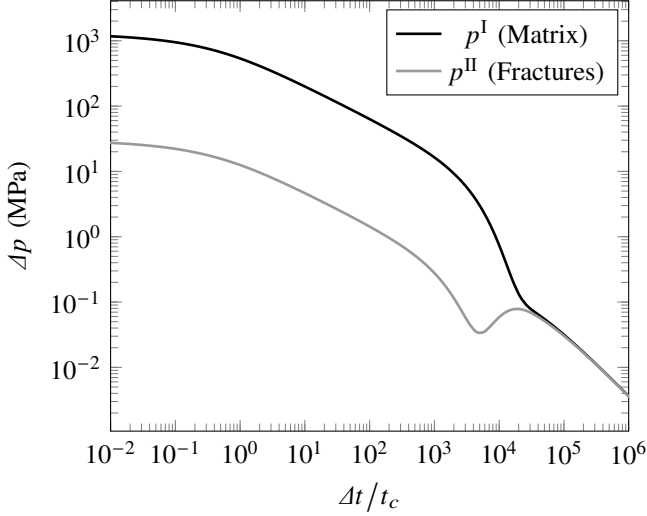


Figure 2. Model validation: assuming Darcy flow in the fractures.

Figure 3 illustrates the after-closure pressure responses derived from the Darcy-flow simulation. In small after-closure time intervals, the pressure within the hydraulic fracture becomes extraordinarily intense, surpassing thresholds that induce significant inertial drag effects.

A. Type Curves

After collecting the flow data, the next step involves conducting simulations incorporating the non-Darcy flow phenomenon within natural fractures. Figure 4 illustrates the disparity in pressure calculations between the Darcy and non-Darcy models, with different parameter values of $\rho\beta\mu^{-1}$, in the non-Darcy modifier.

Considering negative values of the fluid flow rate in the hydraulic fracture, the fracture-pressure responses shown in Figure 4 represent the effects of δ in the semi-analytical model. The term $\rho\beta\mu^{-1}$ in the non-Darcy modifier was set to different values, namely: 1, 3, 10, 15, 20 and 50. The inertial effects due to the presence of the Forchheimer equation in the natural fractures is further observed in the transition zone, where the pressure decline is near to 0 MPa. The pressure decline during the transient period between pseudolinear and pseudoradial flow regimes is anticipated to exhibit a convex trend. Interestingly, the pressure response of the instantaneous point source exhibits negative values within the same time intervals, as show in Figure 3c.

IV. DISCUSSION

A. Effect of Interporosity Coefficient

To investigate additional non-Darcy flow effects, the next simulation focused on selected special cases. Figure 5 illustrates the pressure-decline curves observed when the flow behavior in each medium is considered independently (i.e., $\lambda = 0$). Furthermore, the simulation examines the extreme scenario of infinite-interporosity flow ($\lambda = \infty$), where any pressure difference between the two media balances instantaneously, simulating their behavior as a unified medium.

For $\rho\beta\mu^{-1} = 50$, the behavior of the pressure decline of natural fractures in Figure 5, and in the absence of hydraulic communication, exhibits a markedly greater decline. In scenarios where both media behave as a unified entity ($\lambda = \infty$), the pressure drop of the system reflects solely the behavior observed in the natural fractures. In this case, the overall pressure curve does not fall within the range between the two curves, as would be expected in situations where Darcy flow occurs in both media. This deviation from the expected behavior highlights the distinct nature of natural fractures and their impact on the overall fluid flow dynamics.

B. Apparent Permeability

Based on Forchheimer observations, the deviation from linearity at high flow rates makes the apparent permeability in Darcy's law. The constant Darcy permeability coefficient, k_D can be replaced by a linear function dependent of $\rho q \mu^{-1}$ [1]:

$$\frac{\partial p}{\partial r} = -\frac{\mu}{k_{app}} q, \quad (13)$$

where the apparent permeability is defined with the next linear function:

$$\frac{1}{k_{app}} = \frac{1}{k_D} + \frac{\rho\beta}{\mu k_D} q. \quad (14)$$

This apparent permeability, can be obtained as below:

$$k_{app} = \delta k_D, \quad (15)$$

where δ is the non-Darcy modifier, and its value can be obtained from its average in all regions. The apparent permeability found in every simulation were computed and are shown in Table II.

V. CONCLUSIONS

A fully coupled poroelastic line-source semi-analytical solution is derived. The solution is used to simulate after-closure pressure decline for a hydraulic fracture in a naturally fractured formation under non-Darcy flow. The discussion and analysis suggest:

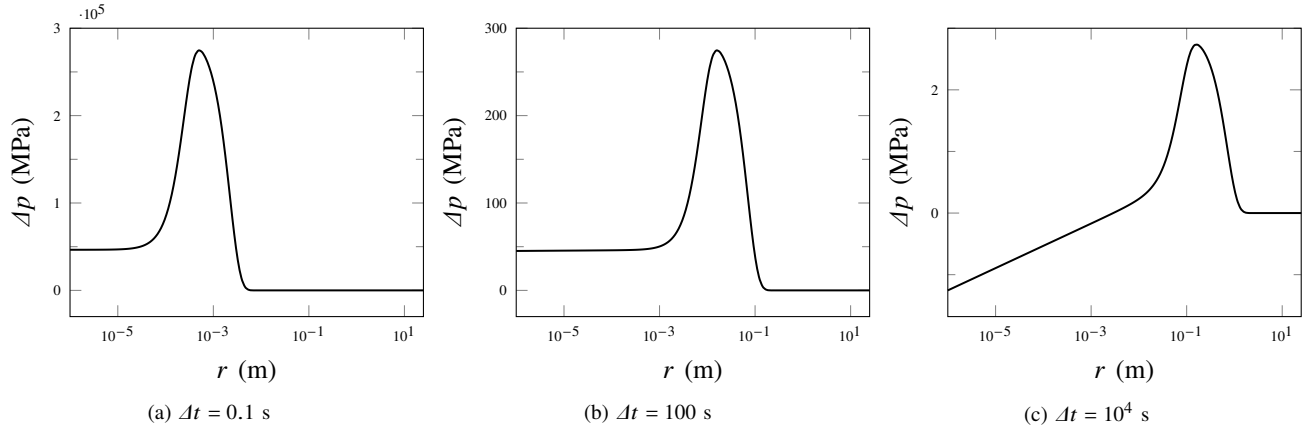


Figure 3. Fracture after-closure pressure response of the point-source solution within the hydraulic fracture at different times.

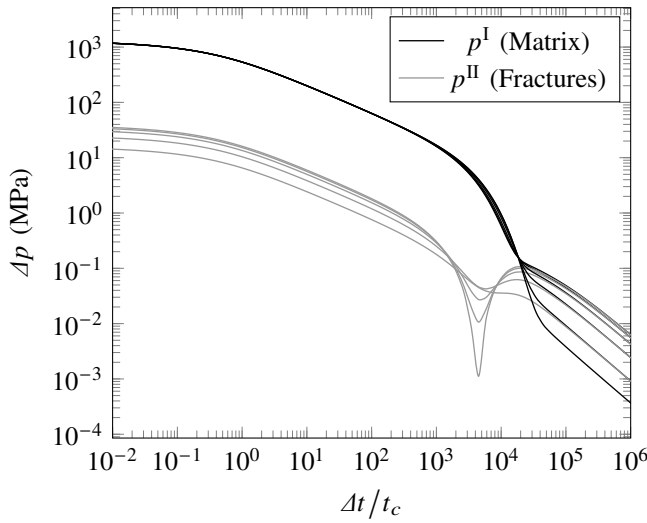


Figure 4. Comparison of pressure decline responses at different values of $\rho\beta\mu^{-1}$.

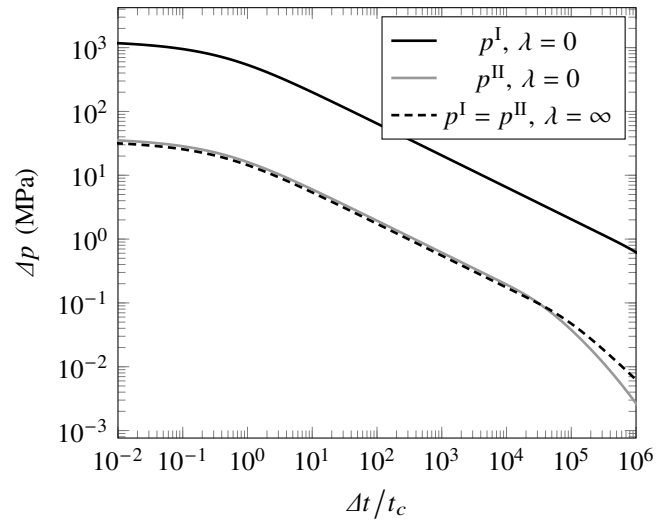


Figure 5. Special cases of the interporosity flow coefficient λ , and effects of non-Darcy flow behavior on p^I and p^{II} .

Table II

APPARENT PERMEABILITY DERIVED FROM THE AVERAGE OF VALUES OF THE NON-DARCY MODIFIER.

	Values					
$\rho\beta\mu^{-1}$ (s m ⁻³)	1	3	10	15	20	500
k_{app} (10 ⁴ nD)	9.99	9.76	9.26	8.92	8.62	2.00

- 1) A non-Darcy modifier is introduced to derive the semi-analytical model, which greatly enhances the accuracy and applicability of our computations for simulation purposes.
- 2) High flow rates were encountered during the initial stages of the impulse fracture test and in the proximity of the wellbore region. These observations strongly indicate the occurrence of inertial effects and validate the necessity of incorporating non-Darcy flow phenomena into the mathematical model.

- 3) The log-log plot of the pressure responses show the significant impact of non-Darcy flow during the transition period, making the pressure decline in the naturally fractures narrower and steeper.
- 4) The examination of special cases of the interporosity coefficient further illustrates the significance of the Forchheimer equation within the mathematical model. These cases provide a deeper understanding of the model's behavior and showcase the specific impact of the Forchheimer term on the pressure response. In particular, it is observed that the pressure decline curves, when the system behaves as a unified system, closely mirror the pressure decline behavior solely attributed to the natural fractures. This emphasizes the important role of the Forchheimer equation in capturing the complex flow dynamics within the naturally fractured media and its ability to accurately represent the pressure decline behavior.

- 5) The calculation of overall apparent permeabilities has yielded valuable insights into the impact of the non-Darcy modifier on the system. The results clearly demonstrate how the inclusion of the non-Darcy term influences the overall flow behavior and permeability estimation.

APPENDIX A
AFTER-CLOSURE WELLBORE PRESSURE CONSIDERING
INTERPOROSITY FLOW

For an infinite domain and irrotational displacement field, the following equation is obtained [9]:

$$\varepsilon = -\frac{\bar{\alpha}^I}{\bar{K} + \frac{4}{3}\bar{G}}p^I - \frac{\bar{\alpha}^{II}}{\bar{K} + \frac{4}{3}\bar{G}}p^{II}. \quad (16)$$

The diffusion equations are obtained substituting (16) into the constitutive equations (Equations (2) and (3)) and the Darcy and non-Darcy flow equations (Equations (4) and (5)) into the fluid continuity equations (Equations (8) and (9)) as follows:

$$\left[\frac{(\bar{\alpha}^I)^2}{\bar{\eta}} + \frac{1}{\bar{M}^I} \right] \frac{\partial p^I}{\partial t} + \left[\frac{\bar{\alpha}^I \bar{\alpha}^{II}}{\bar{\eta}} + \frac{1}{\bar{M}^{I,II}} \right] \frac{\partial p^{II}}{\partial t} = \frac{v^I k^I}{\mu} \nabla^2 p^I + \lambda(p^{II} - p^I), \quad (17)$$

where $\bar{\eta} = \bar{K} + 4\bar{G}/3$. For the flow in the hydraulic fractures, the divergence of the flux is

$$\frac{\partial q_i^{II}}{\partial x_i} = -\frac{k^{II}}{\mu} \frac{\partial}{\partial x_i} \left(\delta \frac{\partial p^{II}}{\partial x_i} \right) \quad (18)$$

where $\delta = (1 + \rho\beta q^{II}/\mu)^{-1}$. And, the diffusion equation is:

$$\left[\frac{\bar{\alpha}^I \bar{\alpha}^{II}}{\bar{\eta}} + \frac{1}{\bar{M}^{I,II}} \right] \frac{\partial p^I}{\partial t} + \left[\frac{(\bar{\alpha}^{II})^2}{\bar{\eta}} + \frac{1}{\bar{M}^{II}} \right] \frac{\partial p^{II}}{\partial t} = \frac{v^{II} k^{II}}{\mu} \frac{\partial}{\partial x_i} \left(\delta \frac{\partial p^{II}}{\partial x_i} \right) - \lambda(p^{II} - p^I). \quad (19)$$

Considering the geometry of the problem, the differential operators can be expressed in polar coordinates. In addition, for a segment i with nodes $i-1$ and i , the non-Darcy modifier $\delta_i(r, t)$ can be approximated by its average $\delta_i(t)$. Therefore, the above system of equations can be expressed in the matrix form for the segment i as:

$$A \frac{\partial}{\partial t} \begin{bmatrix} p^I \\ p^{II} \end{bmatrix} = D \nabla^2 \begin{bmatrix} p^I \\ p^{II} \end{bmatrix} + \Gamma \begin{bmatrix} p^I \\ p^{II} \end{bmatrix}; \quad (20)$$

where

$$A = \begin{bmatrix} \frac{(\bar{\alpha}^I)^2}{\bar{\eta}} + \frac{1}{\bar{M}^I} & \frac{\bar{\alpha}^I \bar{\alpha}^{II}}{\bar{\eta}} + \frac{1}{\bar{M}^{I,II}} \\ \frac{\bar{\alpha}^I \bar{\alpha}^{II}}{\bar{\eta}} + \frac{1}{\bar{M}^{I,II}} & \frac{(\bar{\alpha}^{II})^2}{\bar{\eta}} + \frac{1}{\bar{M}^{II}} \end{bmatrix},$$

$$D = \begin{bmatrix} \frac{v^I k^I}{\mu} & 0 \\ 0 & \frac{v^{II} k^{II}}{\mu} \end{bmatrix}, \Gamma = \lambda \begin{bmatrix} -1 & 1 \\ 1 & -1 \end{bmatrix}.$$

Changing the variable, the system becomes:

$$\frac{\partial}{\partial t} \begin{bmatrix} \zeta^I \\ \zeta^{II} \end{bmatrix} = DA^{-1} \nabla^2 \begin{bmatrix} \zeta^I \\ \zeta^{II} \end{bmatrix} + \Gamma A^{-1} \begin{bmatrix} \zeta^I \\ \zeta^{II} \end{bmatrix}. \quad (21)$$

Then, the pseudo-time is defined over the segment i as:

$$\tau_i = \int_0^t \delta_i(\zeta) d\zeta \quad (22)$$

After applying the Laplace transform to Equation (20) (with respect to τ_i) and using the initial conditions $\zeta^I(\tau_i = 0^+) = \zeta^{II}(\tau_i = 0^+) = 0$ for $r > 0$, the equation can be rewritten in the Laplace domain as follows:

$$\nabla^2 \begin{bmatrix} \tilde{\zeta}^I \\ \tilde{\zeta}^{II} \end{bmatrix} = AD^{-1} (\delta_i s_i I - \Gamma A^{-1}) \begin{bmatrix} \tilde{\zeta}^I \\ \tilde{\zeta}^{II} \end{bmatrix}, \quad (23)$$

where, I stands for the identity matrix, and $s_i N$, the domain parameter.

Equation (23) is a coupled system of partial differential equations that can be solved via eigendecomposition. The solution in matrix form is:

$$\begin{bmatrix} \tilde{\zeta}^I \\ \tilde{\zeta}^{II} \end{bmatrix} = P \begin{bmatrix} C_i^I K_0 \left(\sqrt{\lambda_i^I} r \right) \\ C_i^{II} K_0 \left(\sqrt{\lambda_i^{II}} r \right) \end{bmatrix}. \quad (24)$$

The matrix P satisfies the following condition:

$$P^{-1} AD^{-1} (\delta_i s_i I - \Gamma A^{-1}) P = \begin{bmatrix} \lambda_i^I & 0 \\ 0 & \lambda_i^{II} \end{bmatrix}; \quad (25)$$

where, λ_i^I and λ_i^{II} are the eigenvalues of $AD^{-1} (\delta_i s_i I - \Gamma A^{-1})$, and P is denoted by

$$P = \begin{bmatrix} m_{11,i}^I & m_{12,i}^{II} \\ m_{21,i}^I & m_{22,i}^{II} \end{bmatrix}.$$

The solution must satisfy the instantaneous injection condition in both matrix and fractures. For a unit fluid volume injected at the origin of the infinite plane, the fluid volume must be distributed at a ratio of v^I and v^{II} , and the instantaneous injection condition is:

$$\forall r: \int_0^r \zeta^I 2\pi r dr = v^I, \quad \int_0^r \zeta^{II} 2\pi r dr = v^{II}. \quad (26)$$

Applying the initial value theorem for $r = r_1$, gives solutions for C_1^I and C_1^{II} :

$$\begin{bmatrix} C_1^I \\ C_1^{II} \end{bmatrix} = \begin{bmatrix} b_{11,1}^I & b_{12,1}^{II} \\ b_{21,1}^I & b_{22,1}^{II} \end{bmatrix}^{-1} \begin{bmatrix} v^I \\ v^{II} \end{bmatrix} \quad (27)$$

where;

$$b_{11,1}^I = \lim_{s_1 \rightarrow \infty} \frac{s_1 m_{11,1}^I}{\lambda_1^I}, \quad b_{12,1}^I = \lim_{s_1 \rightarrow \infty} \frac{s_1 m_{12,1}^I}{\lambda_1^I},$$

$$b_{21,1}^I = \lim_{s_1 \rightarrow \infty} \frac{s_1 m_{21,1}^I}{\lambda_1^I}, \quad b_{22,1}^I = \lim_{s_1 \rightarrow \infty} \frac{s_1 m_{22,1}^I}{\lambda_1^I}.$$

Furthermore, the continuity of the variation in volume content requires the next statements:

$$\begin{bmatrix} C_i^I \\ C_i^{II} \end{bmatrix} = \begin{bmatrix} m_{11,i}^I K_0 \left(\sqrt{\lambda_i^I} r_{i-1} \right) & m_{12,i}^I K_0 \left(\sqrt{\lambda_i^I} r_{i-1} \right) \\ m_{21,i}^I K_0 \left(\sqrt{\lambda_i^I} r_{i-1} \right) & m_{22,i}^I K_0 \left(\sqrt{\lambda_i^I} r_{i-1} \right) \end{bmatrix}^{-1} \begin{bmatrix} \xi^I(r_{i-1}) \\ \xi^{II}(r_{i-1}) \end{bmatrix}. \quad (28)$$

A. Instantaneous-Line-Source Solution

The influence of an instantaneous line source with a uniform intensity located at $-L \leq x' \leq L$ can be obtained by integrating the previous point source solution. Specifically, at the origin, the solution in the Laplace domain becomes:

$$\begin{aligned} \tilde{p}_{\text{inst,line}}^I(0,0) = & \sum_{\substack{1 \leq i \leq j \\ r_j=L}} \pi r_i \left\{ n_{11,i}^I C_i^I \left[K_0 \left(\sqrt{\lambda_i^I} r_i \right) L_{-1} \left(\sqrt{\lambda_i^I} r_i \right) \right. \right. \\ & \left. \left. + K_1 \left(\sqrt{\lambda_i^I} r_i \right) L_0 \left(\sqrt{\lambda_i^I} r_i \right) \right] \right. \\ & \left. + n_{12,i}^{II} C_i^{II} \left[K_0 \left(\sqrt{\lambda_i^{II}} r_i \right) L_{-1} \left(\sqrt{\lambda_i^{II}} r_i \right) \right. \right. \\ & \left. \left. + K_1 \left(\sqrt{\lambda_i^{II}} r_i \right) L_0 \left(\sqrt{\lambda_i^{II}} r_i \right) \right] \right\} \\ & - \pi r_{i-1} \left\{ n_{11,i}^I C_i^I \left[K_0 \left(\sqrt{\lambda_i^I} r_{i-1} \right) L_{-1} \left(\sqrt{\lambda_i^I} r_{i-1} \right) \right. \right. \\ & \left. \left. + K_1 \left(\sqrt{\lambda_i^I} r_{i-1} \right) L_0 \left(\sqrt{\lambda_i^I} r_{i-1} \right) \right] \right. \\ & \left. + n_{12,i}^{II} C_i^{II} \left[K_0 \left(\sqrt{\lambda_i^{II}} r_{i-1} \right) L_{-1} \left(\sqrt{\lambda_i^{II}} r_{i-1} \right) \right. \right. \\ & \left. \left. + K_1 \left(\sqrt{\lambda_i^{II}} r_{i-1} \right) L_0 \left(\sqrt{\lambda_i^{II}} r_{i-1} \right) \right] \right\}, \quad (29) \end{aligned}$$

where, L_{-1} and L_0 are the modified Struve functions with orders -1 and 0, respectively [10].

Similarly, the instantaneous line source solution of the pressure in the fractures at the origin is obtained as follows:

$$\begin{aligned} \tilde{p}_{\text{inst,line}}^{II}(0,0) = & \sum_{\substack{1 \leq i \leq j \\ r_j=L}} \pi r_i \left\{ n_{21,i}^I C_i^I \left[K_0 \left(\sqrt{\lambda_i^I} r_i \right) L_{-1} \left(\sqrt{\lambda_i^I} r_i \right) \right. \right. \\ & \left. \left. + K_1 \left(\sqrt{\lambda_i^I} r_i \right) L_0 \left(\sqrt{\lambda_i^I} r_i \right) \right] \right\} \end{aligned}$$

$$\begin{aligned} & + n_{22,i}^{II} C_i^{II} \left[K_0 \left(\sqrt{\lambda_i^{II}} r_i \right) L_{-1} \left(\sqrt{\lambda_i^{II}} r_i \right) \right. \\ & \left. + K_1 \left(\sqrt{\lambda_i^{II}} r_i \right) L_0 \left(\sqrt{\lambda_i^{II}} r_i \right) \right] \right\} \\ & - \pi r_{i-1} \left\{ n_{21,i}^I C_i^I \left[K_0 \left(\sqrt{\lambda_i^I} r_{i-1} \right) L_{-1} \left(\sqrt{\lambda_i^I} r_{i-1} \right) \right. \right. \\ & \left. \left. + K_1 \left(\sqrt{\lambda_i^I} r_{i-1} \right) L_0 \left(\sqrt{\lambda_i^I} r_{i-1} \right) \right] \right. \\ & \left. + n_{22,i}^{II} C_i^{II} \left[K_0 \left(\sqrt{\lambda_i^{II}} r_{i-1} \right) L_{-1} \left(\sqrt{\lambda_i^{II}} r_{i-1} \right) \right. \right. \\ & \left. \left. + K_1 \left(\sqrt{\lambda_i^{II}} r_{i-1} \right) L_0 \left(\sqrt{\lambda_i^{II}} r_{i-1} \right) \right] \right\}. \quad (30) \end{aligned}$$

B. Continuous-Line-Source Solution

If the fluid withdrawal from time 0 to t is at a continuous rate, then the continuous line source solution of the pressure in the matrix at the origin can be expressed as follows:

$$\begin{aligned} \tilde{p}_{\text{cont,line}}^I(0,0) = & \sum_{\substack{1 \leq i \leq j \\ r_j=L}} \frac{\pi r_i}{s_i} \left\{ n_{11,i}^I C_i^I \left[K_0 \left(\sqrt{\lambda_i^I} r_i \right) L_{-1} \left(\sqrt{\lambda_i^I} r_i \right) \right. \right. \\ & \left. \left. + K_1 \left(\sqrt{\lambda_i^I} r_i \right) L_0 \left(\sqrt{\lambda_i^I} r_i \right) \right] \right. \\ & \left. + n_{12,i}^{II} C_i^{II} \left[K_0 \left(\sqrt{\lambda_i^{II}} r_i \right) L_{-1} \left(\sqrt{\lambda_i^{II}} r_i \right) \right. \right. \\ & \left. \left. + K_1 \left(\sqrt{\lambda_i^{II}} r_i \right) L_0 \left(\sqrt{\lambda_i^{II}} r_i \right) \right] \right\} \\ & - \frac{\pi r_{i-1}}{s_i} \left\{ n_{11,i}^I C_i^I \left[K_0 \left(\sqrt{\lambda_i^I} r_{i-1} \right) L_{-1} \left(\sqrt{\lambda_i^I} r_{i-1} \right) \right. \right. \\ & \left. \left. + K_1 \left(\sqrt{\lambda_i^I} r_{i-1} \right) L_0 \left(\sqrt{\lambda_i^I} r_{i-1} \right) \right] \right. \\ & \left. + n_{12,i}^{II} C_i^{II} \left[K_0 \left(\sqrt{\lambda_i^{II}} r_{i-1} \right) L_{-1} \left(\sqrt{\lambda_i^{II}} r_{i-1} \right) \right. \right. \\ & \left. \left. + K_1 \left(\sqrt{\lambda_i^{II}} r_{i-1} \right) L_0 \left(\sqrt{\lambda_i^{II}} r_{i-1} \right) \right] \right\}. \quad (31) \end{aligned}$$

Similarly, the continuous line source solution of the pressure in the fractures at the origin in the Laplace domain is:

$$\begin{aligned} \tilde{p}_{\text{cont,line}}^{II}(0,0) = & \sum_{\substack{1 \leq i \leq j \\ r_j=L}} \frac{\pi r_i}{s_i} \left\{ n_{21,i}^I C_i^I \left[K_0 \left(\sqrt{\lambda_i^I} r_i \right) L_{-1} \left(\sqrt{\lambda_i^I} r_i \right) \right. \right. \\ & \left. \left. + K_1 \left(\sqrt{\lambda_i^I} r_i \right) L_0 \left(\sqrt{\lambda_i^I} r_i \right) \right] \right\} \end{aligned}$$

$$\begin{aligned}
& + n_{22,i}^{\text{II}} C_i^{\text{II}} \left[K_0 \left(\sqrt{\lambda_i^{\text{II}}} r_i \right) L_{-1} \left(\sqrt{\lambda_i^{\text{II}}} r_i \right) \right. \\
& \quad \left. + K_1 \left(\sqrt{\lambda_i^{\text{II}}} r_i \right) L_0 \left(\sqrt{\lambda_i^{\text{II}}} r_i \right) \right] \\
& - \frac{\pi r_{i-1}}{s_i} \left\{ n_{21,i}^{\text{I}} C_i^{\text{I}} \left[K_0 \left(\sqrt{\lambda_i^{\text{I}}} r_{i-1} \right) L_{-1} \left(\sqrt{\lambda_i^{\text{I}}} r_{i-1} \right) \right. \right. \\
& \quad \left. \left. + K_1 \left(\sqrt{\lambda_i^{\text{I}}} r_{i-1} \right) L_0 \left(\sqrt{\lambda_i^{\text{I}}} r_{i-1} \right) \right] \right. \\
& \quad \left. + n_{22,i}^{\text{II}} C_i^{\text{II}} \left[K_0 \left(\sqrt{\lambda_i^{\text{II}}} r_{i-1} \right) L_{-1} \left(\sqrt{\lambda_i^{\text{II}}} r_{i-1} \right) \right. \right. \\
& \quad \left. \left. + K_1 \left(\sqrt{\lambda_i^{\text{II}}} r_{i-1} \right) L_0 \left(\sqrt{\lambda_i^{\text{II}}} r_{i-1} \right) \right] \right\}. \quad (32)
\end{aligned}$$

C. Finite-Interval-Line-Source Solution

For a finite injection of a volume $Q_0 t_p$ with time duration t_c , the after-closure solution for the corresponding pressures are:

$$p_{\text{line,w}}^{\text{I}}(\Delta t) = \frac{Q_0 t_p}{2HL_e t_c} \left[p_{\text{cont,line}}^{\text{I}}(t_c + \Delta t) - p_{\text{cont,line}}^{\text{I}}(\Delta t) \right], \quad (33)$$

$$p_{\text{line,w}}^{\text{II}}(\Delta t) = \frac{Q_0 t_p}{2HL_e t_c} \left[p_{\text{cont,line}}^{\text{II}}(t_c + \Delta t) - p_{\text{cont,line}}^{\text{II}}(\Delta t) \right]. \quad (34)$$

APPENDIX B

CALCULATION OF THE NON-DARCY MODIFIER

Assuming Darcy flow in the fractures, a similar system can be obtained. Therefore, the instantaneous-point-source solution is given as:

$$\begin{bmatrix} \check{p}_{\text{inst,point}}^{\text{I}} \\ \check{p}_{\text{inst,point}}^{\text{II}} \end{bmatrix} = A^{-1} \check{P} \begin{bmatrix} \check{C}^{\text{I}} K_0 \left(\sqrt{\lambda^{\text{I}}} r \right) \\ \check{C}^{\text{II}} K_0 \left(\sqrt{\lambda^{\text{II}}} r \right) \end{bmatrix}, \quad (35)$$

where the check symbol denotes the solutions with Darcy flow in the fractures, and the matrix \check{P} satisfies the following condition:

$$\begin{aligned}
\check{P}^{-1} A \check{D}^{-1} (sI - \Lambda A^{-1}) \check{P} &= \begin{bmatrix} \check{\lambda}^{\text{I}} & 0 \\ 0 & \check{\lambda}^{\text{II}} \end{bmatrix}; \quad A^{-1} \check{P} = \begin{bmatrix} \check{n}_{11}^{\text{I}} & \check{n}_{12}^{\text{II}} \\ \check{n}_{21}^{\text{I}} & \check{n}_{22}^{\text{II}} \end{bmatrix}; \\
\begin{bmatrix} \check{C}^{\text{I}} \\ \check{C}^{\text{II}} \end{bmatrix} &= \frac{1}{2\pi} \begin{bmatrix} \check{b}_{11}^{\text{I}} & \check{b}_{12}^{\text{II}} \\ \check{b}_{21}^{\text{I}} & \check{b}_{22}^{\text{II}} \end{bmatrix}^{-1} \begin{bmatrix} v^{\text{I}} \\ v^{\text{II}} \end{bmatrix}. \quad (36)
\end{aligned}$$

The continuous-line-source solution in the fractures, assuming $r = \sqrt{x^2 + y^2}$ and $y = 0$, is:

$$\begin{aligned}
\check{p}_{\text{cont,line}}^{\text{II}}(r) &= \frac{1}{s} \int_{-L}^L \check{p}_{\text{inst,point}}^{\text{II}}(|x - x'|) dx' \\
&= \frac{1}{s} \int_0^L \check{p}_{\text{inst,point}}^{\text{II}}(|x - x'|) dx' + \frac{1}{s} \int_0^L \check{p}_{\text{inst,point}}^{\text{II}}(x + x') dx' \\
&= \frac{\pi}{2s} \check{n}_{21}^{\text{I}} \check{C}^{\text{I}} \left\{ (L - r) \left[K_0 \left(\sqrt{\lambda^{\text{I}}} (L - r) \right) L_{-1} \left(\sqrt{\lambda^{\text{I}}} (L - r) \right) \right. \right. \\
& \quad \left. \left. + K_1 \left(\sqrt{\lambda^{\text{I}}} (L - r) \right) L_0 \left(\sqrt{\lambda^{\text{I}}} (L - r) \right) \right] \right. \\
& \quad \left. + (L + r) \left[K_0 \left(\sqrt{\lambda^{\text{I}}} (L + r) \right) L_{-1} \left(\sqrt{\lambda^{\text{I}}} (L + r) \right) \right. \right. \\
& \quad \left. \left. + K_1 \left(\sqrt{\lambda^{\text{I}}} (L + r) \right) L_0 \left(\sqrt{\lambda^{\text{I}}} (L + r) \right) \right] \right\} \\
& + \frac{\pi}{2s} \check{n}_{22}^{\text{II}} \check{C}^{\text{II}} \left\{ (L - r) \left[K_0 \left(\sqrt{\lambda^{\text{II}}} (L - r) \right) L_{-1} \left(\sqrt{\lambda^{\text{II}}} (L - r) \right) \right. \right. \\
& \quad \left. \left. + K_1 \left(\sqrt{\lambda^{\text{II}}} (L - r) \right) L_0 \left(\sqrt{\lambda^{\text{II}}} (L - r) \right) \right] \right. \\
& \quad \left. + (L + r) \left[K_0 \left(\sqrt{\lambda^{\text{II}}} (L + r) \right) L_{-1} \left(\sqrt{\lambda^{\text{II}}} (L + r) \right) \right. \right. \\
& \quad \left. \left. + K_1 \left(\sqrt{\lambda^{\text{II}}} (L + r) \right) L_0 \left(\sqrt{\lambda^{\text{II}}} (L + r) \right) \right] \right\}. \quad (37)
\end{aligned}$$

This solution, is used to compute the values of the fluid flux in the fractures over the domain of the line source. The representative value of the non-Darcy modifier in a segment is calculated using the average value of the flux:

$$\begin{aligned}
q_i^{\text{II}} &= -\frac{k^{\text{II}}}{\mu} \cdot \frac{1}{r_i - r_{i-1}} \int_{r_{i-1}}^{r_i} \frac{dp_{\text{inst,point}}^{\text{II}}}{dr} dr \\
&= -\frac{k^{\text{II}}}{\mu} \cdot \frac{p_{\text{inst,point}}^{\text{II}}(r_i) - p_{\text{inst,point}}^{\text{II}}(r_{i-1})}{r_i - r_{i-1}}. \quad (38)
\end{aligned}$$

REFERENCES

- [1] R. D. Barree and M. W. Conway, "Beyond Beta Factors: A Complete Model for Darcy, Forchheimer, and Trans-Forchheimer Flow in Porous Media," in *Presented at the SPE Annual Technical Conference and Exhibition*, 09 2004, paper SPE-89325-MS, doi: 10.2118/89325-MS.
- [2] E. Choi, T. Cheema, and M. Islam, "A new dual-porosity/dual-permeability model with non-darcian flow through fractures," *Journal of Petroleum Science and Engineering*, vol. 17, no. 3, pp. 331–344, 1997, doi: 10.1016/S0920-4105(96)00050-2.
- [3] Y.-S. Wu, "Numerical simulation of single-phase and multiphase non-darcy flow in porous and fractured reservoirs," *Transport in Porous Media*, vol. 49, no. 2, pp. 209–240, 11 2002, doi: 10.1023/A:1016018020180.
- [4] S. Al-Rbeawi and J. F. Owayed, "Fluid flux throughout matrix-fracture interface: Discretizing hydraulic fractures for coupling matrix darcy flow and fractures non-darcy flow," *Journal of Natural Gas Science and Engineering*, vol. 73, p. 103061, 2020, doi: 10.1016/j.jngse.2019.103061.
- [5] C. Liu, A. Mehrabian, and Y. N. Abousleiman, "Poroeleastic dual-porosity/dual-permeability after-closure pressure-curves analysis in hydraulic fracturing," *SPE Journal*, vol. 22, no. 01, pp. 198–218, 06 2016, doi: 10.2118/181748-PA.
- [6] F. Zeng, G. Zhao, and X. Xu, "Transient Pressure Behaviour Under Non- Darcy Flow, Formation Damage and Their Combined Effect for Dual Porosity Reservoirs," *Journal of Canadian Petroleum Technology*, vol. 48, no. 07, pp. 54–65, 07 2009, doi: 10.2118/09-07-54.
- [7] J. Bear, *Modeling Phenomena of Flow and Transport in Porous Media*, 1st ed., ser. Theory and Applications of Transport in Porous Media. Springer, 2018, no. 31, doi: 10.1007/978-3-319-72826-1.
- [8] F. Zeng, "Modeling of non-Darcy flow in porous media and its application," PhD dissertation, Faculty of Graduate Studies and Research, 2008. [Online]. Available: <http://hdl.handle.net/10294/14202>
- [9] C. Liu, "Poroeleastic After-Closure Pressure Decline Analysis In Dual-Porosity Dual-Permeability Formations," PhD dissertation, Mewbourne College of Earth and Energy, 2016. [Online]. Available: <https://hdl.handle.net/11244/34655>
- [10] Besselk. The Mathematical Functions Site. Identification number: 03.04.21.0004.01. [Online]. Available: <http://functions.wolfram.com/03.04.21.0004.01>